TOMOGRAPHIC SEPARATION OF COMPOSITE SPECTRA. I. THE COMPONENTS OF PLASKETT'S STAR

WILLIAM G. BAGNUOLO, JR., DOUGLAS R. GIES,
and MICHAEL S. WIGGS

Center for High Angular Resolution Astronomy
Department of Physics and Astronomy, Georgia State University, Atlanta, GA 30303

p. 36

Running Title: The Components of Plaskett's Star

Received ______________________________

Address all editorial correspondence to:

William G. Bagnuolo, Jr.
Center for High Angular Resolution Astronomy
Department of Physics and Astronomy
Georgia State University
Atlanta, GA 30303-3083

ABSTRACT

We have analyzed the UV photospheric lines of Plaskett's Star (HD 47129), a 14.4 day period, double-lined O-type spectroscopic binary. Archival data from *IUE* (17 spectra well distributed in orbital phase) were analyzed with several techniques. A cross-correlation analysis, which showed that the secondary produces significant lines in the UV, indicates that the mass ratio is $q = 1.18 \pm 0.12$ (secondary slightly more massive). A tomography algorithm was used to produce the separate spectra of the two stars in six spectral regions. The interpolated spectral classifications of the primary and secondary, O7.3 I and O6.2 I, respectively, were estimated through a comparison of UV line ratios with those in spectral standard stars. The intensity ratio of the stars in the UV is 0.53 ± 0.05 (primary brighter). The secondary has a strong P Cygni N IV λ 1718 feature, indicating a strong stellar wind. The secondary lines appear rotationally broadened, and we estimate the projected rotational velocity $V \sin i$ for this star to be 310 ± 20 km s^{-1}. We discuss the possible evolutionary history of this system through a comparison of the positions of the components and evolutionary tracks in the H-R diagram.

Subject headings: Stars: binaries – Stars: individual (HD 47129, Plaskett's Star) – Ultraviolet: spectra

1. INTRODUCTION

Plaskett's Star, or HD 47129, has generally been considered the most massive binary since its discovery in 1922 ($f(M) = 12.6 M_{\odot}$; Stickland 1987), yet in many ways it is still poorly understood. The spectral type of the primary has been classified variously as an O7.5 III(f) by Garmany, Conti, & Massey (1980), O7 I by Hutchings & Cowley (1976), and O8p by Walborn (1972). The radial velocity curve of the primary from both visual and UV lines is well determined (Stickland 1987). The secondary, on the other hand, has always been an enigma. Because the lines of the secondary are weak and diffuse, its classification is still uncertain. Similarly, orbit determinations based on the radial velocity of the secondary lines are difficult because of the large velocity fluctuations of some of these lines. Plaskett (1922) derived $K_2 = 246.7$ km s^{-1} and $q = M_s/M_p = 0.84$ (primary more massive), based mainly on the He II λ 4542 and 4200 lines, and the He I λ 4026, 4472, 4713, and 4922 lines. According to Plaskett, the secondary has a slightly earlier spectral type. Struve (1948) noted that the systemic velocity, γ, of his radial velocity curve for the secondary was systematically smaller than that for the the primary by 100 km s^{-1}, and he was uncertain as to whether any of the observed features could actually be attributed to the secondary component. Struve, Sahade, & Huang (1958) thought that the secondary might be more massive ($K_2 < K_1$), and also presented a hypothesis that the secondary is actually a cooler A-type star that is locally heated by the primary to mimic an O-type spectrum. This idea was further explored by Sahade (1962), who also estimated that $q = 1.25$. More recently, Hutchings & Cowley (1976) inferred nearly the same spectral type for the secondary as for the primary (O7 I), and estimated a mass ratio of $q = 1.0 \pm 0.1$. Both Heap (1981) and Stickland (1987) were unable to see the secondary lines in the UV in spectra obtained from the *International Ultraviolet Explorer Satellite (IUE)*. These authors believe therefore that the secondary might be an O-star but somewhat later in type than the primary.

In a previous paper (Bagnuolo & Gies 1991) we analyzed the UV photospheric spectra of the O-type binary AO Cas. Archival data from 16 spectra uniformly distributed in orbital phase from *IUE* were analyzed with a tomography algorithm to produce the separate spectra of the two stars in six spectral regions. The spectral classifications of the primary and secondary, O9.5 III and O8 V, respectively, were estimated through a comparison of UV line ratios with those in spectral standard stars. We also estimated the intensity ratio to be in the range 0.5-0.7 (primary brighter) at 1600 Å. Tomography appears to be an extremely useful technique for studying the spectra and the physical properties of both the primary and especially the less luminous secondary components of binary systems.

Because of the apparent utility of the analysis of the AO Cas ultraviolet spectra, we undertook a similar analysis of Plaskett's Star. The history of the interpretation of Plaskett's Star, particularly of the spectral type and radial velocity curve of the secondary, suggests that the best results are obtained by measuring lines with high excitation. Because the UV photospheric lines form in higher excitation transitions than the optical lines, they are less prone to contamination from circumstellar emission components. In the following sections of this paper we apply several analyses to *IUE* high resolution spectra of Plaskett's Star. By means of a cross-correlation technique we first attempt to estimate independently the mass ratio, q, of the star (§2). We then apply a tomography algorithm to the set of spectra to obtain the separated spectra and thus the spectral types of the components (§3). By further analyzing the separated spectra we then estimate the UV intensity ratio of the components and also the rotational velocity of the secondary (§4).

2. CROSS-CORRELATION ANALYSIS AND MASS RATIO

The ultraviolet spectra were gathered from the *IUE* Regional Data Analysis Facility in

Boulder. The details of the processing of the *IUE* data are given in a previous paper by Gies & Wiggs (1991). Seventeen of the 19 spectra listed by Stickland (1987) were used (SWP 2360 and 3236 were omitted). Data were extracted in the vicinity of Si IV λ1400, C IV λ1550, He II λ1640, and N IV λ1718, the features described in Gies & Wiggs (1991). For this tomographic analysis, we selected six spectral regions, two each from the larger S IV λ1400 and C IV λ1550 regions (on either side of these stellar wind lines), and the entire He II λ1640 and N IV λ1718 regions. The UV spectra were smoothed to reduce noise by convolving the spectra with a Gaussian function with a FWHM = 3 pixels (approximately 0.15 Å). The spectra were transformed to a uniform, heliocentric velocity grid, with a pixel spacing of 10 km s^{-1}, and the velocity registration of each spectrum was altered so that the positions of the interstellar lines matched their positions in a mean global spectrum. The wavelength scale ranges from 0.0467 Å pixel^{-1} (Region 1349-1379 Å) to 0.0574 Å pixel^{-1} (Region 1663-1774 Å). Interstellar line features at λ1370.3, 1526.8 (Si II), 1608.5 (Fe II), 1656.5, 1656.9 (C I), 1670.7, 1741.6 (Ni II), and 1752.1 were removed from the data by interpolation.

The cross-correlation analysis was based on that described in Gies & Wiggs (1991) for AO Cas. We extracted three sub-regions in the data for cross-correlation analysis: 1360-76, 1413-33, and 1607-51 Å. The selection of these regions was based on a preliminary spectral typing (see §3) that indicated that the secondary is slightly earlier in type and had relatively strong lines (mainly Fe V and He II) in these regions. We chose a "single-lined" spectrum obtained near orbital phase 0.25 or superior conjunction of the primary (SWP 4774, taken at orbital phase 0.264) as a reference spectrum that was cross-correlated with each of the seventeen individual spectra. The normalized cross-correlations for each spectral region were added together, with weights of 0.5, 0.25, 1.00 respectively, based on a preliminary goodness of fit estimate. The composite cross-correlation data, 201 velocity points $\times$ 17 spectra, were then rectified to unit intensity by fitting a straight line through the values at the velocity extrema.

We made an initial estimate of the relative radial velocity of the secondary by fitting the cross-correlation data with two Gaussian functions to represent the contributions of both stars. The velocity registration of the Gaussian for the primary was set according to the circular orbit of Stickland (1987), but the widths of both Gaussians, the relative amplitude of the Gaussians, and the position of the secondary Gaussian were left as fitting parameters. The best-fitting set of parameters yielded estimates of the radial velocities of the secondary, which we then fit by a sinusoid using a least-squares technique to find the mass ratio. This method gave a mass ratio of about $q = 1.5$, but this is very probably an overestimate.

The 'single lined' spectrum that we used for cross-correlation has line profiles with extended wings that are largely due to the secondary. Consequently, the cross-correlation functions will be convolutions of the primary and secondary spectra with a composite reference spectrum. Failure to include realistic wings in the fitting function for the 'primary' line in the cross-correlation functions will result in the fitted secondary line moving closer to the primary, thus producing a lower measured radial velocity difference and a higher secondary mass. We therefore repeated the analysis with a more realistic 'primary' line for the cross-correlation, one generated by taking sixteen of the cross-correlations (omitting the cross-correlation of the reference with itself) and performing a tomographic separation of components. The shapes of the 'primary' and 'secondary' lines derived varied only slowly with assumed mass-ratios of 1.0 to 1.4. Figure 1 shows these 'lines' derived from the cross-correlation functions, assuming a mass ratio of 1.0 and a 'line' intensity ratio of 0.7. These profiles represent the convolutions of the reference spectrum with the primary and secondary spectra, respectively.

We then made a new attempt at deriving secondary velocities from the cross-correlation functions by substituting the individual, tomographically separated functions for the Gaussian functions used in our first try. The function corresponding to the primary was symmetrized about the dip minimum (this averaging produced a slightly better fit to the data), and this function was shifted in velocity according to Stickland's (1987) velocity curve. We then fit the individual composite cross-correlation functions by shifting the secondary function in velocity and varying the intensity ratio of primary to secondary line depth to achieve the best fit. Two forms were tried for the secondary function, a broad Gaussian (with fitted width) and the estimated tomographic shape, shown in Figure 1. Assuming, as previously, a broad Gaussian for the 'secondary' line of the cross-correlation resulted in velocities that yielded a mass-ratio $q = 1.23$. (A circular orbit and sinusoidal radial velocities were assumed.) Assuming the tomographic shape (from bottom of Figure 1 and symmetrized) resulted in a mass ratio of $q = 1.18$. Using the tomographic shape function for the secondary function gave a 10% better fit in terms of χ^2 than using the Gaussian, but otherwise the results were very similar. Table 1 shows the results for the individual secondary radial velocity fits for the tomographic secondary shape function. Figure 2A shows the run of cross-correlation functions with phase and the fits to them from the tomographic secondary shape. Note the clear presence of the secondary component. Figure 2B shows the estimated lines in the cross-correlation functions due to the secondary only, created by subtracting the fitted primary line. Note that the secondary line feature is evident throughout the orbit.

If the secondary were an A-type star with one hemisphere heated by the companion to O-type temperatures (Struve, Sahade, & Huang 1958), then the secondary component would only appear dominant at orbital phases when the heated hemisphere was oriented toward us (between phases 0.5 and 0.0 with a maximum at phase 0.75). Instead, we find that the secondary contribution to the cross-correlation functions is relatively constant with orbital phase, which implies that the secondary must have an O-type spectrum throughout the orbital cycle.

Figure 3 shows the radial velocity curve for the secondary, which was fitted by least-squares assuming a circular orbit. Two outlier points, (SWP 10048 and SWP 2626, shown as open circles), which had comparatively weak cross-correlation minima, were omitted in calculating the radial velocity amplitude. The errors in mass ratio can be estimated from the propagation of errors in the curve fit (discussed by Bevington 1969, p. 154) and were consistently about 10% for various fits. (This analysis conservatively included the two outlier points.) Thus, our estimate for the mass ratio of Plaskett's Star is $q = 1.18 \pm 0.12$. Because of the observed lack of eclipses, the inclination i must be less than roughly $i = 70°$. (Our estimates of the primary and secondary radii from §4 give a limit of $i = 69.3°$ - $72.7°$, depending on the secondary radius.) The lower limit for inclination (and upper limit on the masses) is not as clearcut, but Rudy & Herman (1978) estimate $i = 71° \pm 9°$ from polarimetry, and comparisons of the stars' location the H-R diagram with evolutionary tracks also suggest that the inclination cannot be too much lower than 70°. Assuming $i = 65°$ to $75°$ (Hutchings & Cowley 1976), $f(M) = 12.60\ M_\odot$ from Stickland (1987), and $q = 1.1$ to 1.3, the range of most probable star masses are 44 to 62 $M_\odot$ for the secondary and 34 to 56 $M_\odot$ for the primary. For $q = 1.2$ and $i = 70°$, the most likely masses for secondary and primary are 51.0 and 42.5 $M_\odot$ respectively.

3. SPECTRAL TYPES OF THE PRIMARY AND SECONDARY

We have discussed the use of a modified version of the ILST tomography algorithm for separating the spectra of binary stars in a previous paper (Bagnuolo & Gies 1991, hereafter referred to as BG). The following briefly summarizes our methodology. A binary star can be represented by a luminous 'object' two pixels thick by n pixels long, where n is the number of pixels per spectrum (or two $1 \times n$ spectral 'objects' bonded together). Due to the radial velocity differences of the stars, a number of view angles for tomography are generated in which parallel rays traverse the 'object' and impinge on a detector, producing the observed spectra at a given orbital phase.

In BG we describe the general formulation of the ILST (Iterative Least Squares Technique) and its application to separating binary star spectra. Basically, the ILST algorithm takes the set of all rays that include a given cell i and computes the difference between the observed ray intensities and the computed ones using the intensity estimates of the previous iteration. The sum of the differences, weighted appropriately, allows an improved estimate of the intensity at i. For the specific case of binary star spectra, the 'object' has dimensions $2 \times n$, and let $f_{1,i}$ and $f_{2,i}$ represent the spectra of the primary and secondary respectively, where i ranges from 1 to n, the length of the spectrum. Then, the incremental corrections to the intensity are calculated using

$$\Delta f_{1,i} = \delta \times \frac{\sum_{k=1}^{m} p_{k,i} - \left[f_{1,i} + f_{2,i+s_k}\right]}{m} \tag{1a}$$

$$\Delta f_{2,i} = r\delta \times \frac{\sum_{k=1}^{m} p_{k,i-s_k} - \left[f_{1,i-s_k} + f_{2,i}\right]}{m} \tag{1b}$$

where $p_{k,i}$ is the i^{th} pixel of the k^{th} binary spectrum of a set of m spectra, and s_k is the radial velocity shift of secondary spectrum relative to primary for the k^{th} spectrum. For this purpose, all the spectra were transformed in velocity to the reference frame of the primary star. The initial spectra can be either single-lined or flat spectra; the spectrum assumed for the secondary is scaled by the assumed intensity ratio r. The parameter δ is a damping factor, and in our reconstructions any δ in the range 0.3 to 0.8 reached a satisfactory convergent solution.

The separated individual spectra of the two stars in each of the six regions were produced by the modified ILST algorithm described above, and they appear in Figures 4 to 9b. These results are from 150 iterations, although little change was noted after 50 iterations. A mass ratio of $q = 1.2$ was assumed. (Assumed mass ratios of 1.0 to 1.4 lead to only small differences in the reconstructed spectra.) An intensity ratio of $r = 0.50$ was assumed, based on a preliminary analysis described below. Thirty-eight pixels at either end are omitted from these reconstructed spectra to avoid edge effects.

Spectral classifications of the two stars for each spectral region were estimated through comparison with standard spectra in the *International Ultraviolet Explorer Atlas of O-Type Spectra from 1200 to 1900 Å*, (Walborn, Nichols-Bohlin, & Panek 1985, hereafter referred to as "the O-star Atlas") and with the spectral sequence of Walborn and Panek (1984). Additional line identifications were derived from Bruhweiler, Kondo, & McCluskey (1981) and McCluskey & Kondo (1981). To better facilitate comparison with the O-star Atlas, plots were made with the x-axes compressed to match the aspect ratio of spectra in the Atlas.

A preliminary typing of the stars was done using the spectral features in each region described below with four supergiant stars in the O-star Atlas [O6 I(n)fp (λ Cep), O6.5 Iaf (HD 163758), O7.5 Iaf (9 Sge), and O8 Iaf (HD 151804)]. The following are the results of these classifications:

<u>Region 1349-1379 Å</u> (Figure 4). This region is dominated by Fe V lines ($\lambda\lambda$1361, 1363, 1366, 1371, 1373, 1376) which strengthen from B0 to O6. The pseudo-continuum "hill" at 1368 Å strengthens in intensity from O9.5 through O7.5. In the primary the relative strengths of the Fe V lines are compatible with O6.5 Iaf (HD 163758), O7.5 Iaf (9 Sge) or O8 Iaf (HD

151804), with 9 Sge providing a slightly better match. The secondary lines appear blended by rotational broadening, but the Fe V lines are also strong. The overall appearence is like O6 I(n)fp (λ Cep), which has some blended Fe V lines in the range 1363-5 Å and some distinct lines in the range 1370-80 Å.

Region 1412-1438 Å (Figure 5). Fe V and C III lines are prominent in this region. The main features are Fe V $\lambda\lambda$1430, 1429, C III at $\lambda\lambda$1426, 1428, and the Fe V blend around 1420 Å. The Fe V λ1430 line strengthens compared to C III $\lambda\lambda$1426, 1428 from B0 through O5. The Fe V λ1420 blend strengthens relative to surroundings from B0 to about O7.5. Based on these criteria, particularly the relative strengths of the Fe V and C III lines, the primary spectrum is matched best with O7.5 Iaf (9 Sge), and, to a slightly lesser extent, with O6.5 Iaf (HD 163758). The secondary is best matched by O6 I(n)fp (λ Cep) and by O6.5 Iaf (HD163758) (if its lines were further rotationally broadened).

Region 1498-1528 Å (Figure 6). This is a nondescript region with few outstanding features. The feature at λ1502, a blend of several high-ionization metal lines (Walborn & Panek 1984), appears much stronger in the secondary than the primary spectrum. This feature is deeper between O5 to O6.5 than at O7.5, and the "hill" at 1522 Å has a greater intensity at the earlier types. These two features are also stronger in class I than class III. The relative strengths of these features indicate that the secondary is about a subclass earlier in spectral type than the primary. The best matches to the primary and secondary spectra are O7.5 Iaf (9 Sge), and O6.5 Iaf (HD 163758) respectively.

Region 1565-1598 Å (Figure 7). This region has primarily Fe IV lines and the so-called λ1574 emission feature (see the O-Star Atlas). The best fit to the primary is O7.5 Iaf (9 Sge); the next best O6.5 Iaf (HD 163758). The best fit to the secondary is O6.5 Iaf (HD 163758) and the second best is O6 I(n)fp (λ Cep) .

Region 1587-1693 Å (Figures 8a,b). This large region contains Fe IV lines and the prominent He II λ1640 line. The region has been plotted in two segments to maintain a wavelength scale consistent with the other plots. The best fit to the primary in Figure 8a is O6.5 Iaf (HD 163758) , which provides a slightly better fit than O7.5 Iaf (9 Sge). In Figure 8b, the λ1640: λ1647 ratio also favors the former, but for the rest of this figure, both these stars are equally good fits to the primary. In Figures 8a and 8b the secondary is about equally well fit by O6 I(n)fp (λ Cep) and O6.5 Iaf (HD 163758) . The 'normal' appearence of the He II line definitely rules out a secondary of type O5 or earlier.

Region 1663-1774 Å (Figures 9a,b). This region contains primarily lines of Fe IV and

N IV (especially the large N IV λ1718 feature) and N III (λ 1748-51). The best fit to the primary is O7.5 Iaf (9 Sge); the next best fit is O6.5 Iaf (HD 163758). The best fit to the secondary is O6.5 Iaf (HD 163758) and to a lesser extent O6 I(n)fp (λ Cep). Note the strong P Cygni profile of the secondary, which indicates that the secondary has a surprisingly strong stellar wind. In a later paper (Wiggs & Gies 1991), the stellar wind features of Plaskett's Star will be analyzed in detail.

The best overall estimate of the interpolated spectral types of the primary and secondary stars are O7.2 I and O6.2 I, respectively, based on a weighted average for the six regions. In these estimates the stars mentioned as "best fit" were weighted 1.0 and those mentioned as "next best" were weighted 0.5.

Because the luminosity class of the primary has been variously estimated to be type I (Hutchings & Cowley 1976; Heap 1981), or type III (Howarth & Prinja 1989; Conti & Leep 1974), we expanded the list of spectral standard stars from the O-star Atlas to sixteen. The fits of the primary spectrum to the comparison stars were rated on a scale of 0 (very poor), 1 (fair), 2 (good), and 3 (excellent) for each of the regions, with the large regions 1587-1693 Å and 1663-1774 Å subdivided into two halves. Spectral features that show luminosity effects at O6.5 (and generally to a lesser extent at O7.5) are: Fe V $\lambda\lambda$1426-30 and C III lines (weaker in supergiants), the λ1502 line and λ1520 feature (stronger), the λ1574 emission feature (weaker), the Fe IV λ1588 line blend (stronger), the appearence of lines near the He II λ1640 line, the strength of the N IV λ1718 feature (stronger), and the strength of the N III λ1748-52 lines compared to nearby Fe IV lines. Because of the possibility of colliding winds with radial velocities not related to either star, we could not use the strong wind features described in the O-star Atlas for luminosity classification. (Indeed, as noted in §2, we selected regions avoiding the Si IV λ1400 and C IV λ1550 wind features.) Most of the features listed as luminosity discriminants above have been previously noted in the cited references on stellar classification, but the use of the 'new' lines $\lambda\lambda$1502, 1520, and 1588 for this purpose seemed justified by the suite of stars in the O-star Atlas.

Table 2A gives these cumulative scores. The best fits to the primary, in order of goodness of fit, are: O7.5 Iaf (9 Sge, score 18.5), O7.5 II((f)) (HD 162978, score 14.0), O7 Ib(f) (HD 192639), score 13.5), O7 II(f) (HD 34656, score 13.5), O7.5 III((f)) (HD 186980, score 13.0), O7 II(f) (HD 151515, score 11.0), and O6.5 Iaf (HD 163758, score 10.0). In Table 2B, which lists the cumulative scores as a function of spectral type and luminosity class, it is evident that luminosity class I generally appears to fit the data better than luminosity class III. The interpolated spectral type for the primary appears to be about O7.3 I.

We also considered luminosity effects for the secondary spectrum. At spectral type

O6.5 luminosity effects are more pronounced than at O7.5. The fits to the secondary are: O6 I(n)fp (λ Cep, score 16.0), O6.5 Iaf (HD 163758, score 13.0), O6.5 Ib(f) (HD 69464, score 6.0), O6.5 III(f) HD 190864, score 4.0), O7.5 Iaf (9 Sge, score 2.5), and O5 If (HD 14947, score 2.0). The best estimate of the secondary spectral type is again O6.2 I. The secondary tends to be fit much better by luminosity class I than less luminous classes.

The type we derive for the primary is thus close to that estimated by Hutchings & Cowley (1976). Our estimated secondary type is about one subclass earlier than the primary. These results rule out the recent "conventional wisdom" that the secondary is a somewhat later type O-star than the primary, but instead confirm Plaskett's original surmise.

4. THE PHYSICAL PROPERTIES OF THE STARS

To better understand the evolutionary state of the stars, we need to estimate their temperatures, intensity ratio in the UV, and individual luminosities. Given the interpolated spectral types adopted here for the primary and secondary of O7.3 I and O6.2 I, respectively, the temperatures are 35.1 and 38.4 kK respectively, using Howarth & Prinja's (1989) calibration. The corresponding bolometric corrections are -3.41 and -3.67, respectively, for the two stars.

We can estimate the individual luminosities in two ways: i) use the estimated distance from its suggested membership in the association Mon OB2 (Humphries 1978), and ii) derive estimates of the radii from the mass and surface gravities. For the first method, we first need the relative intensity of the stars to derive the individual magnitudes from the combined magnitude. The intensity ratios of the stars can best be estimated from the equivalent widths of distinct spectral lines or clusters of lines in the spectra of the primary and the secondary. It is evident from equations (1) that the intensity ratio is a required input parameter for the ILST reconstruction algorithm if there are no lines with zero intensity, because otherwise the algorithm could converge to a spurious solution in which (say) a constant intensity is added to the primary star spectrum and simultaneously subtracted from the secondary star spectrum. For lines that do not approach zero intensity, as is clearly the case in Plaskett's Star, we need a method similar to Petrie's (1939), which is also described by Abhyankar (1959). Let A_1 and A_2 be the equivalent widths of a spectral line in the reconstructed primary and secondary spectrum, respectively. Let r be the assumed intensity ratio used for the reconstruction. Then the relative continuum intensities of the two spectra are $1/(1+r)$ and $r/(1+r)$, respectively, and the absolute line strengths are $s_1 = A_1/(1+r)$ and $s_2 = rA_2/(1+r)$. If r_t is the true intensity ratio, and if the strength of the lines is the same in each star, then $s_2 = r_t s_1$, and thus $r_t = rA_2/A_1$. Note that equivalent widths are needed instead of line depths because of the difference in rotational broadening of the stars.

For this analysis we chose twelve lines or line blends at the following features: $\lambda\lambda$1361-3-5 (Fe V), 1374 (Fe V), 1420 (Fe V), 1525 (Fe IV), 1584 (Fe IV + Fe V), 1592 (Fe IV), 1640 (He II), 1647 (Fe IV), 1681 (Fe IV), 1688 (N IV + Fe IV), 1747 (N III), and 1752 (N III). Of these lines, given the spectral classifications of primary and secondary, the Fe IV lines are expected to be relatively weaker in the secondary, but the He II, Fe V, and N IV lines are expected to be stronger. Because of this diverse collection of lines and because the spectral types differ by only a subclass, we do not expect much systematic bias in determining the true intensity ratio. Assuming an initial intensity ratio of 0.5 leads to an average line area ratio A_2/A_1 of 1.042 $\pm$0.053. (The line ratio is 1.063 if we double weight the strong He II line.) This gives a true intensity ratio of 0.52 - 0.53, and we assume the latter. As a check on methodology, this process was repeated assuming an initial intensity ratio of 0.40, and this produced an estimate of the true intensity ratio of 0.50. Because of the possibility of systematic effects in line selection, we conservatively double the nominal error, and thus we estimate the intensity ratio of the stars near 1600 Å to be $r = 0.53 \pm 0.05$. By using Kurucz (1979) model atmospheres we can estimate the magnitude difference in V between the stars. By using interpolation from two flux models ($T_{\rm eff}$ = 35,000 and 40,000 K with $\log g$= 4.0, the lowest gravity model at 40,000 K) we find a color difference between the stars at 0.07 magnitudes between 1608 Å and 5470 Å, *i.e.*, if $\Delta m_{UV} = 0.69$, then $\Delta m_V = 0.76$. By comparison, a black-body estimate shows a color difference of 0.11 magnitudes. (It should be remembered that even 1600 Å is solidly in the Rayleigh-Jeans part of the black-body curve.)

We can use the distance modulus of 10.89, a V extinction of $A_V = 1.11$, and a visual magnitude of 6.05 (Humphries 1978) to estimate the bolometric magnitudes for the primary and secondary to be -8.93 and -8.43, respectively, and thus $\log L/L_\odot = 5.47$ and 5.27, respectively. Similarly, the radii can be estimated at 14.7 and 9.7 $R_\odot$, respectively. In Figure 10 we plot the locations of the components of Plaskett's Star in the H-R diagram with the stellar evolutionary tracks of Maeder & Meynet (1988). The location of the primary in Figure 10 suggests that the star started out with a mass of roughly 35 $M_\odot$ (and currently has a mass of ≈ 30 $M_\odot$). Thus our estimated mass (≈ 42.5 $M_\odot$), and the luminosity class (I, corresponding to $\log L/L_\odot \approx 5.9$; Howarth & Prinja 1989), are incompatible with the evolutionary mass and estimated luminosity of this star of $\log L/L_\odot = 5.47$. Because we believe that the masses and luminosity classes are probably better established for Plaskett's Star than the luminosities based on distance and extinction, we next examine the estimates of the latter.

The extinction and especially the distance appear to be rather poorly known. The value of A_V listed by Humphries (1978) was estimated from $E(B-V)$ using a value for the ratio of total to selective extinction $R_V = 3.0$, and it is now known that values of R_V as high as 5.5 exist (Cardelli, Clayton, & Mathis 1989, hereafter referred to as CCM89). To estimate R_V, we compared the spectrophotometric data of Plaskett's Star from the *Ultraviolet Bright-Star*

Spectrophotometric Catalogue (Jamar *et al.* 1976) with the Kurucz model most appropriate for the primary ($T_{\rm eff}$ = 35,000 K, $\log g$= 3.5) to obtain an estimate of the change in extinction ΔA_λ from 1410 to 2737 Å. We also included an estimate of the flux in V. The resultant extinction curve (assuming several values of A_V) could be compared to the three curves in Fig. 4 of CCM89 showing A_λ/A_V as a function of $1/\lambda$ for stars with R_V = 2.75, 3.52, and 5.30. Unfortunately, the data are compatible with a large range of R_V from 2.7 to 3.7, and therefore do not shed much light on this problem (although they do rule out very large values of R_V). The best current estimate of R_V for a star near Plaskett's Star is R_V=3.52 for HD 48099 (CCM89). If this value were adopted for Plaskett's Star, the extinction would be revised moderately upward to A_V=1.30, instead of 1.11.

The distance modulus of Plaskett's Star is perhaps more uncertain, because our line of sight is directed into a greatly foreshortened spiral arm (Morgan *et al.* 1965). Previous distance determinations of Plaskett's Star have depended on several assumptions: i) the star is physically related to the 'ring' in the association Mon OB2 and has the same distance, ii) the ring is at the same distance as NGC 2244, the central cluster of the association Mon OB2, and iii) the distance determination of NGC 2244. All these assumptions are subject to some error. The evidence for (i) is not completely convincing, given that the star is some 0.5° from the ring center. Furthermore, five stars known to be in Mon OB2 (HD 46149, 46150, 46223, 46573, 46966) have radial velocities of 41.1, 38.8, 41.1, 38.1, and 35.6 km s^{-1}, respectively (Gies 1987). The average radial velocity of these stars, 38.9 km s^{-1}, is sufficiently different from the systemic (γ) radial velocity of Plaskett's Star, 23.0 km s^{-1}, (Stickland 1987) to raise some doubt about the latter's membership in Mon OB2. (HD 48099 has a radial velocity of 11.0 km s^{-1}, and may or may not be associated with the ring.) The uncertainty in the distance of the 'ring' has been discussed by Conti & Alschuler (1971). Finally, estimates of the distance to Mon OB2 itself have varied, ranging from 800 pc (Morgan *et al.* 1965), 1660 pc (Johnson 1962) and 2200 pc (Becker & Fenkart 1963), to the more recent estimate of 1590 pc (Turner 1976). In short, the distance to Plaskett's Star is uncertain. Hopefully, binary star measurements with an interferometer with a baseline of > 200 m (e.g. McAlister, Bagnuolo, & Hartkopf 1990) will provide precise astrometric orbits and distances for systems like Plaskett's Star.

We can estimate the luminosities in another way by finding the radii through an examination of the surface gravities of the stars. The various criteria that are applied to determine luminosity class reflect the photospheric pressure and hence the surface gravity in the stellar atmosphere. Thus we have referred to several non-LTE line profile studies of O-type supergiants described in the review of Kudritzki & Hummer (1990) to determine $\log g$ values appropriate to the components of Plaskett's Star. Based on stars of similar classification we estimate that $\log g$ = 3.4 ± 0.2 and 3.5 ± 0.2 for the primary and secondary, respectively. Then we can combine our estimates of $T_{\rm eff}$ (from spectral type), masses (from §2), and surface gravities to arrive at luminosities of $\log L/L_\odot = 5.80 \pm 0.2$ and 5.94 ± 0.2 for the primary and secondary, respectively.

The physical properties of the stars for these luminosities are listed in Table 3, and the positions in the H-R diagram are shown in Figure 10. The primary now appears as a fairly normal supergiant with an initial mass of 54 $M_\odot$ and a current mass of $\approx$ 42 $M_\odot$. Adopting the primary's luminosity and the intensity ratio derived above yields a combined absolute magnitude of $M_V = -6.78$, and for $A_V = 1.30$, the inferred distance is 2020 pc, well beyond the distance of Mon OB2 (1510 pc). Thus, the supergiant classification of the primary evidently rules out membership in the Mon OB2 association.

The high luminosity derived for the secondary star apparently contradicts the fainter UV intensity ratio described above. If we instead rely on the UV intensity ratio to determine the relative sizes of the stars, then a different luminosity for the secondary results. We used the flux tables of Kurucz (1979) interpolated to the appropriate temperatures and gravities of the stars to determine a surface flux ratio at 1608 Å between the stars, and using the observed flux ratio we derive a radius ratio of $R_s/R_p = 0.64$ (assuming similar limb darkening laws). If we adopt the luminosity and radius of the primary star given in Table 3, then the secondary radius is 13.8 $R_\odot$ and the luminosity is reduced to $\log L/L_\odot = 5.57$. This lower luminosity estimate is also shown in Figure 10. If the secondary is this small, then the surface gravity is $\log g = 3.9$, a value more appropriate to luminosity class III - V stars.

The resolution to this apparent conflict in secondary luminosity derived from the luminosity class and the UV flux ratio probably can be found in the rapid rotation of the secondary. Because the system's inclination ($i \approx 70°$) favors an equatorial view of the star, its rapid rotation and consequent gravity darkening will cause us to underestimate the surface averaged temperature and bolometric luminosity, so that the luminosity derived from the UV intensity ratio will be a lower limit. For similar reasons, our luminosity class estimate may be biased toward the lower photospheric pressures found near the equator, and therefore our luminosity estimate based on $\log g$ represents an upper limit.

Because the stars are similar in spectral type, we can estimate the projected rotational velocity of the secondary by convolving the sharper-lined primary lines with a rotational broadening function. In our reduction program a region of interest is selected, broadened with a rotational broadening function with a limb-darkening coefficient of 0.464, and normalized to match those of the secondary in strength. This limb darkening coefficient is estimated from Wade & Rucinski (1985) for a wavelength of 1625 Å and $T_{\rm eff}$ = 35,000 K, $\log g = 3.5$. The assumed projected rotational velocity, $V \sin i$, is adjusted to obtain the minimum χ^2. We chose four regions (1352.7-1376.4, 1567.6-1595.5, 1594.3-1687.3, and 1670.0-1766.7 Å), which yielded estimates of $V \sin i$ of 306, 266, 296, and 317 km s^{-1}, respectively. The relative weights of the four regions were determined from the second deriviative of χ^2 with velocity (Bevington 1969) to be 1.6, 1.5, 5.4, and 4.0, and the overall estimate of $V \sin i$ is therefore 300 $\pm$15 km s^{-1}. Finally, this value must be adjusted to include the effect of the finite width of the primary line. Assuming a rotational velocity of 75 km s^{-1} (Conti & Ebbets 1977) for the primary results in a final estimated $V \sin i$ of the secondary of 310 km s^{-1}.

We also used the cross-correlation results plotted in Figure 1 to obtain a rough estimate of the rotational velocity of the primary. The FWHM of the sharp-lined feature at the top of Figure 1, which corresponds to the autocorrelation of the primary lines, is about 220 km s^{-1} wide, which corresponds very roughly to a rotational velocity of $\approx$ 78 km s^{-1}, in agreement with the 75 km s^{-1} found by Conti & Ebbets (1977). Given the estimated radii, inclination, and period, the synchronous rotational velocities of the primary and secondary are 71 and 46-70 km s^{-1} respectively. Thus, while the primary may be rotating at close to the synchronous rate, this is far from the case for the secondary. The secondary has a projected rotational velocity which is close to the maximum observed velocity among O-type supergiants (Conti & Ebbets 1977), and thus the deformation and gravity darkening of the star must be substantial. Collins & Sonneborn (1977) and Slettebak, Kuzma, & Collins (1980) have discussed the effects of rapid rotation for stars as early as B0. Because these effects are nonlinear and haven't apparently been computed for O-stars, we will not pursue this matter further in this paper, but we note that rotational effects could explain much of the apparent underluminosity of this star.

One final constraint on the luminosity of the secondary star is provided by its stellar wind characteristics. We found that the N IV λ1718 feature appeared as a regular absorption line in the spectrum of the primary, but as a well developed, P Cygni wind profile in the spectrum of the secondary. This suggests that the mass loss rate of the secondary equals or exceeds that of the primary. Since the mass loss rate depends fundamentally on luminosity (Howarth & Prinja 1989), this suggests that the luminosity of the secondary is similar to or slightly greater than the luminosity of the primary.

Finally, it is tempting to speculate on the evolutionary history of the components of Plaskett's Star. Two plausible scenarios can be imagined that incorporate the large rotational velocity of the secondary. In the simplest case, the two stars could be core hydrogen burning objects evolving off the main sequence. The primary star has evolved like a single star of initial mass $\approx 54 M_{\odot}$, while the secondary has followed the track of a star with an initial mass of $\approx 60 M_{\odot}$. In this scenario, the rapid rotation of the secondary has slowed down its redward evolution in the H-R diagram due to enhanced mixing of extra hydrogen into the core. A second, perhaps equally plausible, scenario is that the system represents an Algol-type stage in evolution in which the primary was initially the more massive star, but through evolutionary expansion it subsequently filled its Roche volume and transferred mass to the companion (the secondary), reversing the mass ratio. Suppose that the primary started with an initial mass of 60 $M_{\odot}$, passed the first temperature minimum or point 5 on Maeder & Meynet's (1988) evolutionary track, and is currently in an blueward evolving phase. This star would have reached a radius of 53 $R_{\odot}$, which exceeds the current Roche radius of $\approx$ 41 $R_{\odot}$ (Eggleton 1983). The star would have transferred both mass and angular momentum to the secondary through Roche lobe overflow, and the now more massive secondary could have been spun up to the large rotational velocity we currently observe. A definitive test of these two scenarios may be possible through a comparison of high S/N spectroscopic observations of the secondary in the UV and optical with realistic models of rapidly rotating O-type supergiants.

We wish to acknowledge T. Meylan, J. Gallagher, W. Hartkopf, H. McAlister, and K. Kamper for useful criticism. One of us (WGB) has been partially supported by NSF grant AST 89-16110. DRG gratefully acknowledges the financial support of the NASA Astrophysics Data Program Grant NAG 5-1218.

TABLE 1

OBSERVED SECONDARY RADIAL VELOCITIES

Orbital Phase	Image No. (SWP)	V_r (observed) (km s^{-1})	V_r (calculated) (km s^{-1})	$O-C$ (km s^{-1})
0.008	3347	-182.3	-172.4	-9.9
0.075	10048	(-4)	-153.8	...
0.264	4774	-25.9	15.2	-41.1
0.279	2516	-3.2	31.3	-52.4
0.337	6369	111.1	89.7	21.3
0.400	4797	128.5	139.7	-11.2
0.437	9950	144.5	159.3	-14.8
0.522	4819	189.1	171.0	18.1
0.552	2626	(45)	163.4	...
0.591	7077	155.9	145.2	10.7
0.674	10089	111.5	79.3	32.2
0.676	10152	94.4	77.4	17.0
0.700	6438	36.0	53.3	-17.3
0.866	6295	-106.6	-115.0	8.4
0.916	13964	-173.8	-149.1	-24.6
0.981	8867	-166.6	-171.4	4.8
0.983	8868	-134.1	-171.6	37.6

TABLE 2A

PRIMARY STAR SPECTRAL CLASSIFICATION

Spectral Classification	Name	Similarity Score
O6 I(n)fp	λ Cep	1.0
O6.5 Iaf	HD 163758	10.0
O7.5 Iaf	9 Sge	18.5
O8 Iaf	HD 151804	7.0
O6.5 Ib(f)	HD 69464	6.0
O7 Ib(f)	HD 192639	13.5
O7 Ib(f)	HD 193514	9.0
O7 II(f)	HD 34656	13.5
O7 II(f)	HD 151515	11.0
O7.5 II ((f))	HD 162978	14.0
O8 II((f))	HD 175754	6.5
O6 III(f)	HD 93130	2.0
O6.5 III(f)	HD 190864	5.5
O7.5 III((f))	HD 186980	13.0
O7.5 III((f))	ξ Per	6.0
O6.5 V((f))	HD 93146	3.5

TABLE 2B

PRIMARY STAR SPECTRAL CLASSIFICATION - SUMMARY

Spectral Type	Luminosity Class Ia	Ib	II	III	V
O6	1.0	...	...	2.0	...
O6.5	10.0	6.0	...	5.5	3.5
O7	...	11.2	12.2	...	...
O7.5	18.5	...	14.0	9.5	...
O8	7.0	...	6.5	...	...

TABLE 3

COMPONENTS OF PLASKETT'S STAR

Parameter	Primary	Secondary
$M/M_\odot$	42.5	51.0
Interpolated Spectral Classification	O7.3 I	O6.2 I
$T_{\rm eff}$	35,100 K	38,400 K
$\log L/L_\odot$	5.80	5.57 – 5.94
$R/R_\odot$	21.5	13.8 – 21.1
$\log g$	3.4	3.5 – 3.9
$V \sin i$ (km s^{-1})	75	310

REFERENCES

Abhyankar, K. D. 1959, ApJS, 4, 157

Bagnuolo, W. G., Jr. & Gies, D. R. 1991, ApJ (to appear July 20 1991)

Becker, W. & Fenkart, R. 1963, Zs. f. Ap., 56, 257

Bevington, P. R. 1969. *Data Reduction and Error Analysis for the Physical Sciences* (New York: McGraw-Hill)

Bruhweiler, F. C., Kondo, Y., & McCluskey, G. E. 1981, ApJS, 46, 255

Cardelli, J. A., Clayton, G. C., & Mathis, J. S. 1989, ApJ, 345, 245

Collins, G. W., II, & Sonneborn, G. H. 1977, ApJS, 34, 41

Conti, P. S., & Alschuler, W. R. 1971, ApJ, 170, 335

Conti, P. S., & Ebbets, D. 1977, ApJ, 213, 438

Conti, P. S., & Leep, E. M. 1974, ApJ, 193, 111

Eggleton, P. P. 1983, ApJ, 268, 368

Garmany, C. D., Conti, P. S., & Massey, P. 1980, ApJ, 242, 1063

Gies, D. R. 1987, ApJS, 64, 545

Gies, D. R., & Wiggs, M. S. 1990, ApJ (to appear July 1 1991)

Heap, S. R. 1981, in *The Universe at Ultraviolet Wavelengths. The First Two Years of International Ultraviolet Explorer*, NASA CP-2171, ed. R. D. Chapman (Washington: NASA), p. 485

Howarth, I. D., & Prinja, R. K. 1989, ApJS, 69, 527

Humphries, R. M. 1978, APJS, 38, 309

Hutchings, J. B., & Cowley, A. P. 1976, ApJ, 206, 490

Jamar, C., Marcau-Hercot, D., Monfils, A., Thompson, G. I., Houziaux, L., & Wilson, R. 1976, *Ultraviolet Bright-Star Spectrophotometric Catalogue*, SR-27, (Paris: ESA)

Johnson, H. L. 1962, ApJ, 136, 1135

Kudritzki, R. P., & Hummer, D. G. 1990, ARA&A, 28, 303

Kurucz, R. L. 1979, ApJS, 40, 1

Maeder, A., & Meynet, G. 1988, A&AS, 76, 411

McAlister, H. A., Bagnuolo, W. G., Jr., & Hartkopf, W. I. 1990, SPIE Proceedings, Vol. 1237, *Amplitude and Intensity Spatial Interferometry*, p. 22

McCluskey, G. E., & Kondo, Y. 1981, ApJ, 246, 464

Morgan, W. W., Hiltner, W. A., Neff, J. S., Garrison, R., & Osterbrock, D. E. 1965, ApJ, 142, 974

Petrie, R. M. 1939, Pub. Dom. Ap. Obs. Victoria, 7, 205

Plaskett, J. S. 1922, MNRAS, 82, 447

Rudy, R. J., & Herman, L. C. 1978, PASP, 90, 163

Sahade, J. 1962, in *Symposium on Stellar Evolution*, La Plata Obs., Argentina, p. 191

Slettebak, A., Kuzma, T. J. & Collins, G. .W.,II 1980, ApJ, 242, 171

Stickland, D. J. 1987, Observatory, 107, 68

Struve, O. 1948, ApJ, 107, 327

Struve, O., Sahade, J., & Huang, S.-S. 1958, ApJ, 127, 148

Turner, D. G. 1976, ApJ, 210, 65

Wade, R. A., & Rucinski, S. M. 1985, A&AS, 60, 471

Walborn, N. R. 1972, AJ, 77, 972

Walborn, N. R., & Panek, R. J. 1984, ApJ, 286, 718

Walborn, N. R., Nichols-Bohlin, J., & Panek, R. J. 1985, *International Ultraviolet Explorer Atlas of O-Type Spectra from 1200 to 1900 Å*, NASA RP-1155 (Washington: NASA)

Wiggs, M. S., & Gies, D. R. 1991, in preparation

FIGURE CAPTIONS

FIG. 1.– Estimates from tomography of the primary (*top*) and secondary (*bottom*) 'line' features in the cross-correlation functions plotted against relative radial velocity. The upper plot is offset by one unit for clarity. These curves represent the convolution of the line profiles in the reference spectrum (obtained near inferior conjunction of the primary) with the line profiles of the primary (*top*) and secondary (*bottom*), respectively.

FIG. 2a.–*Upper Frame*: Cross-correlation functions of the UV spectra with a single-lined, conjunction phase spectrum plotted against relative radial velocity (*solid lines*). The profiles are arranged in order of increasing orbital phase and each function is placed in the y-ordinate so that the continuum equals the phase of observation (phase 0.25 = superior conjunction of the primary). The bar in the upper right gives the intensity scale relative to a unit continuum. Superimposed on each function is the fit (*dotted lines*) constructed from the line features in Fig. 1. *Lower Frame*: A gray-scale representation of the orbital variations in the cross-correlation functions. Here each cross-correlation intensity is assigned one of sixteen gray levels based on its value between the minimum (dark) and maximum (bright) observed values. The shape of the function at each phase in the image is calculated by a linear interpolation between the closest observed phases. The portions of the image for the first and last 20% of the orbit are reproduced at the bottom and the top of the image, respectively, to improve the sense of phase continuity. The solid white lines over-plotted in the gray-scale image show the velocity curves of the primary (from Stickland 1987) and the secondary (based on a mass ratio $q = 1.18$).

FIG. 2b.–Plaskett's Star cross-correlation functions for the secondary alone, constructed by subtraction of the model primary lines. (Same format as Fig. 2a.)

FIG. 3.–The radial velocity of the secondary star from the cross-correlation fits as a function of orbital phase. The solid lines represent a sinusoidal fit to the secondary velocities assuming a circular orbit, and the circular orbit of the primary (Stickland 1987). Two observations (*open circles*) were omitted from the fit.

FIG. 4.–Spectra of the primary (*top*) and secondary (*below*) components of Plaskett's Star, from tomography of 17 *IUE* spectra, in Region 1349-1379 Å. Both spectra are rectified to unit continuum (here defined as the maximum intensity in the region). For clarity the primary spectrum is offset by one unit.

FIG. 5.–Spectra of the primary (*top*) and secondary (*bottom*) components of Plaskett's Star in Region 1412-1438 Å.

FIG. 6.–Spectra of the primary (*top*) and secondary (*bottom*) components of Plaskett's Star in Region 1498-1528 Å.

FIG. 7.–Spectra of the primary (*top*) and secondary (*bottom*) components of Plaskett's Star in Region 1565-1598 Å.

FIG. 8a.–Spectra of the primary (*top*) and secondary (*bottom*) components of Plaskett's Star in Region 1587-1693 Å (first half).

FIG. 8b.–Spectra of the primary (*top*) and secondary (*bottom*) components of Plaskett's Star in Region 1587-1693 Å (second half).

FIG. 9a.–Spectra of the primary (*top*) and secondary (*bottom*) components of Plaskett's Star in Region 1663-1774 Å (first half).

FIG. 9b.–Spectra of the primary (*top*) and secondary (*bottom*) components of Plaskett's Star in Region 1663-1774 Å (second half).

FIG. 10.–The estimated temperature and luminosity of the primary and secondary components of Plaskett's Star compared to the evolutionary tracks of Maeder & Meynet (1988) labeled by the initial masses. Open circles: initial estimates (from membership in Mon OB2); filled circles: revised estimates (based on spectral properties). The two limits for the luminosity of the secondary are connected by a solid line.

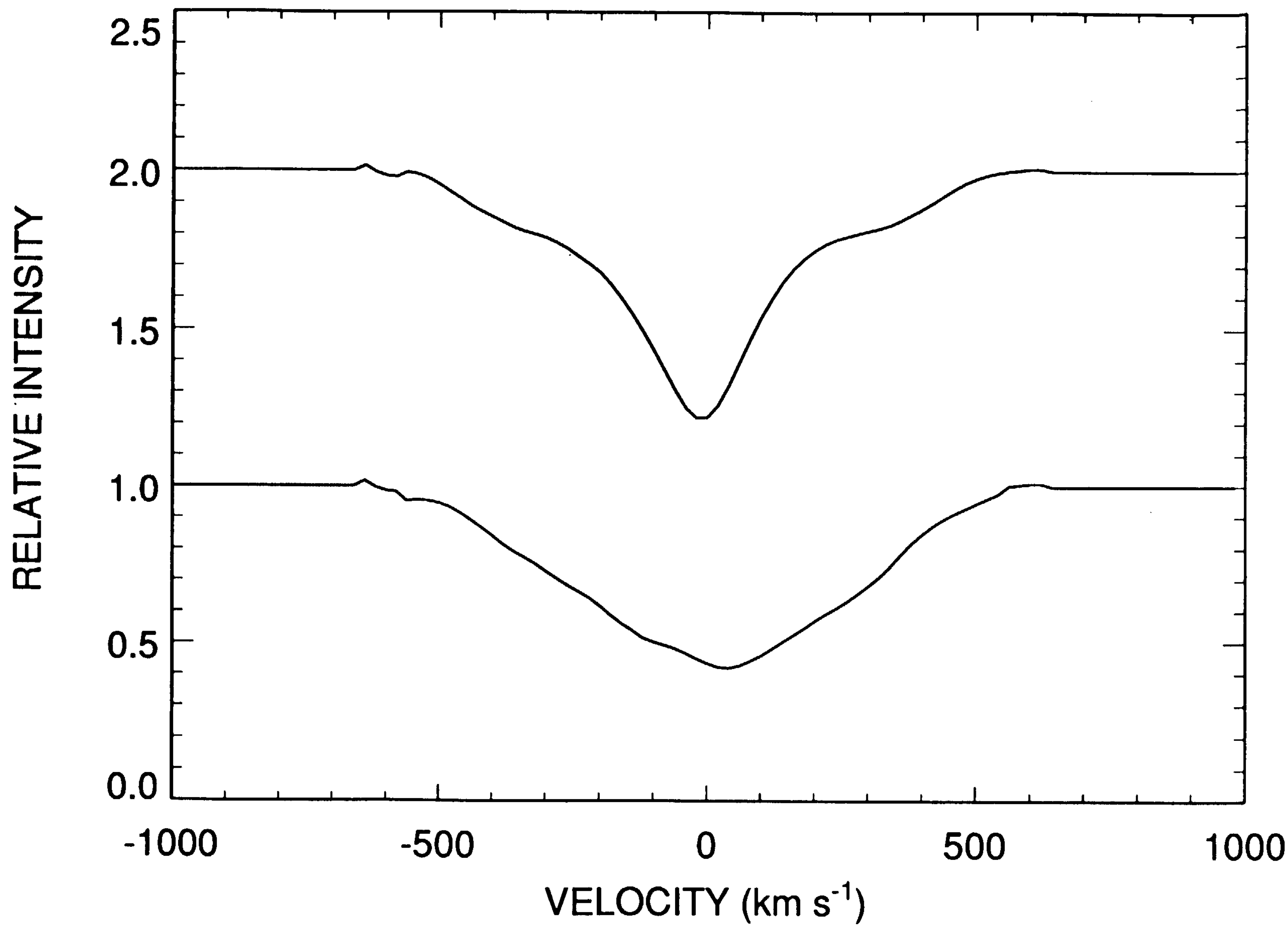
2.5
2.0
1.5
1.0
0.5
0.0
RELATIVE INTENSITY
-1000
-500
0
500
1000
VELOCITY (km s-1)

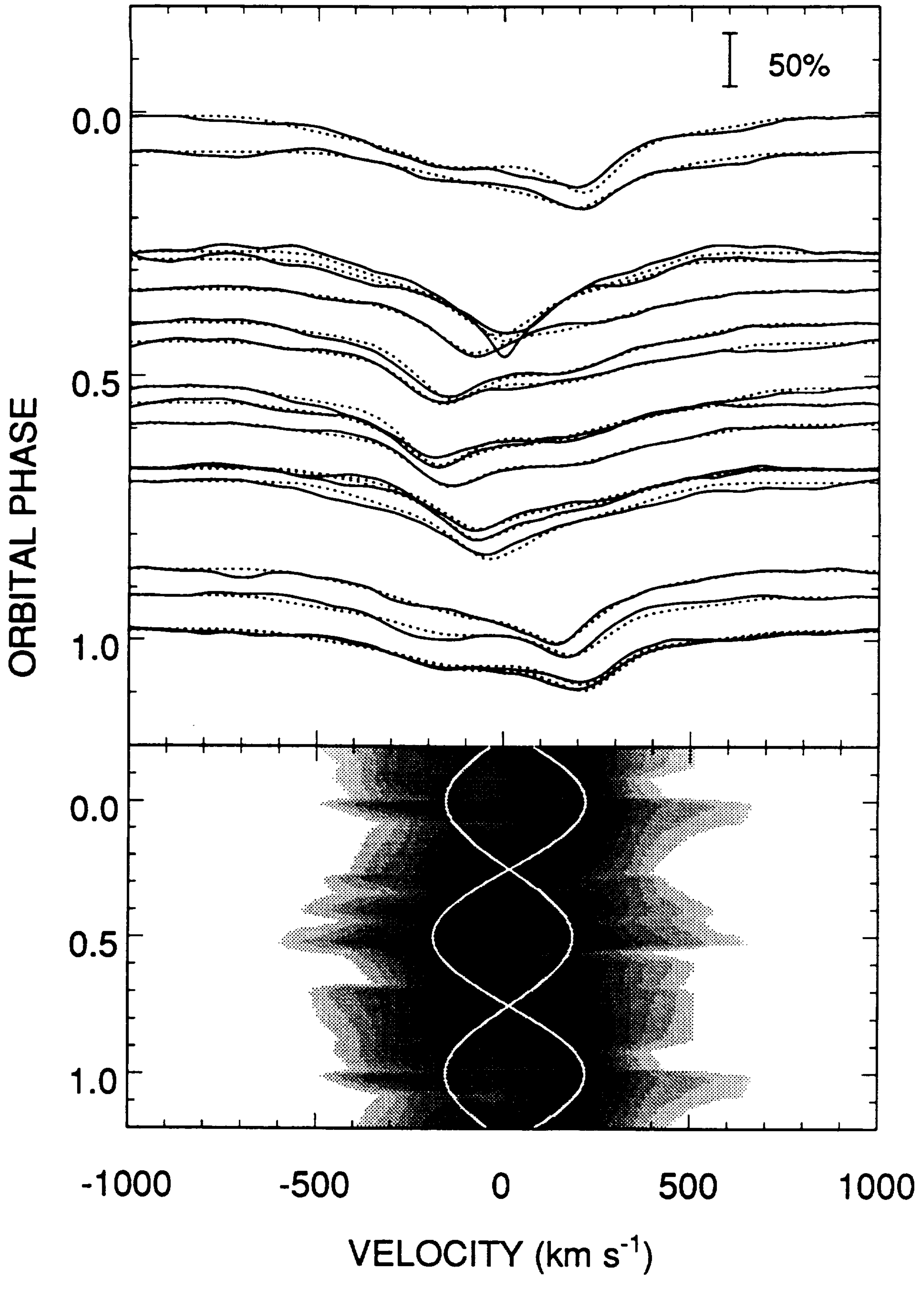

50%
ORBITAL PHASE
0.0
0.5
1.0
0.0
0.5
1.0
-1000
-500
0
500
1000
VELOCITY (km s-1)

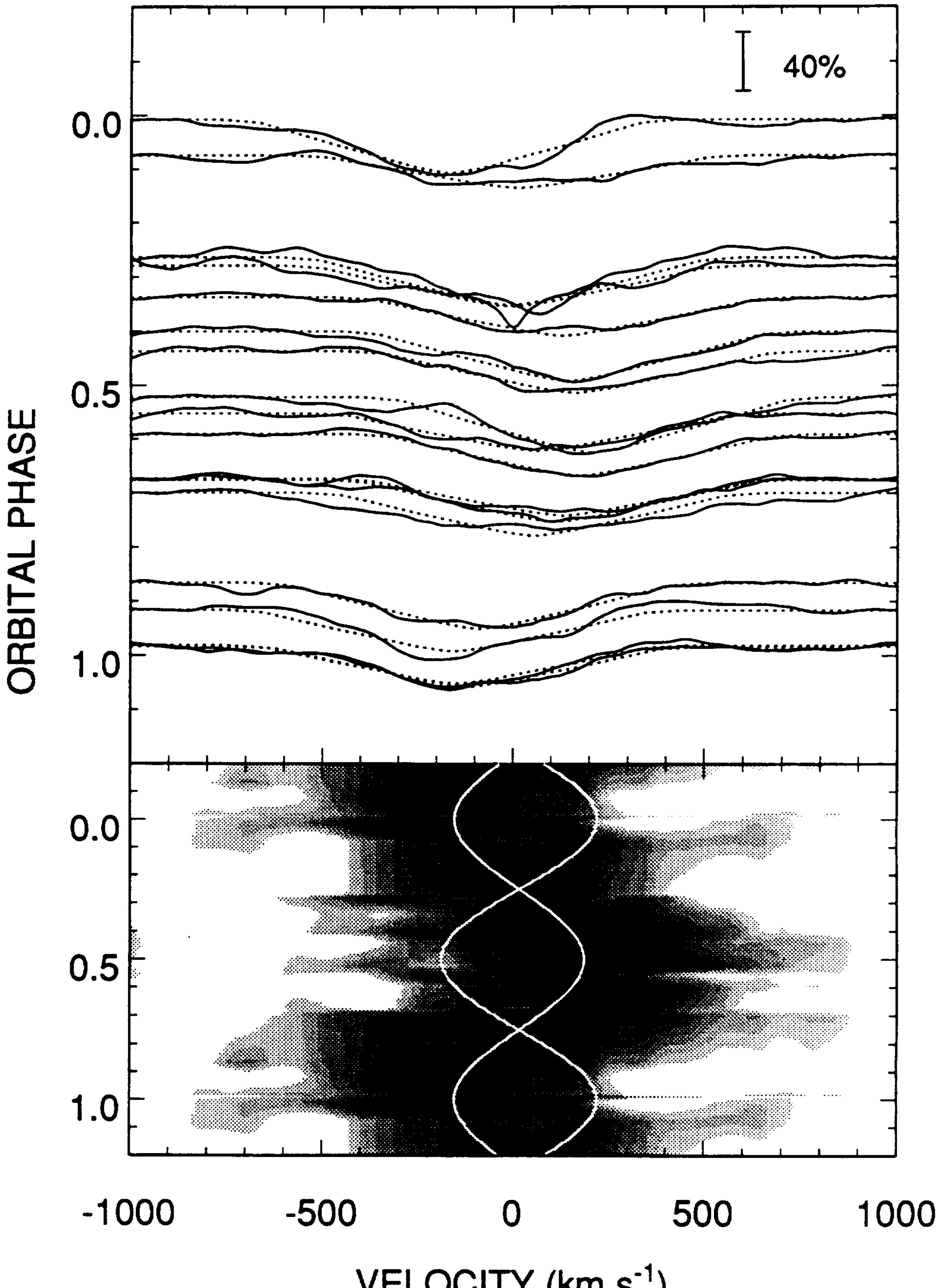

40%
0.0
0.5
1.0
ORBITAL PHASE
0.0
0.5
1.0
-1000
-500
0
500
1000
VELOCITY (km s^{-1})

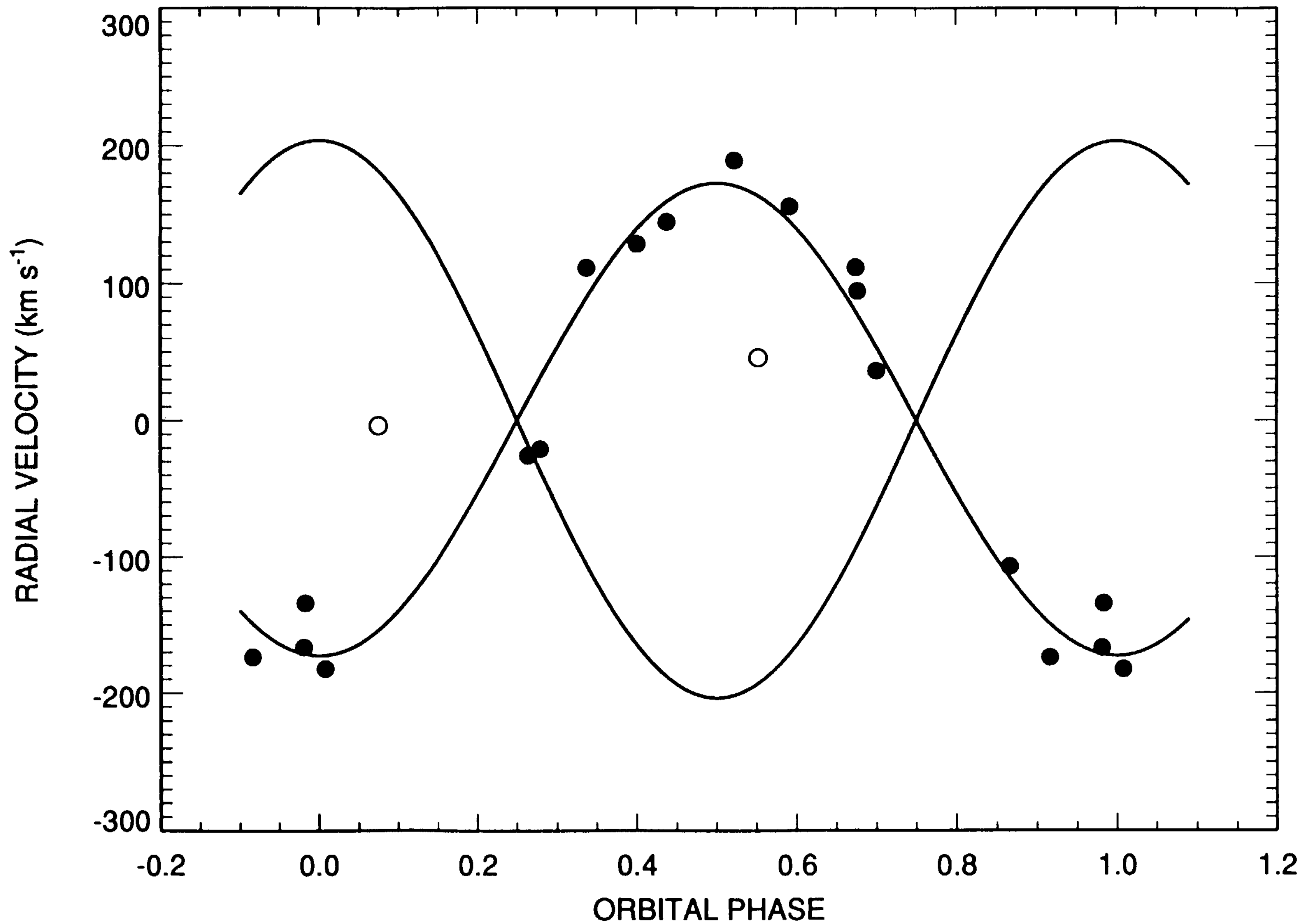
RADIAL VELOCITY (km s^{-1})
ORBITAL PHASE
300
200
100
0
-100
-200
-300
-0.2
0.0
0.2
0.4
0.6
0.8
1.0
1.2

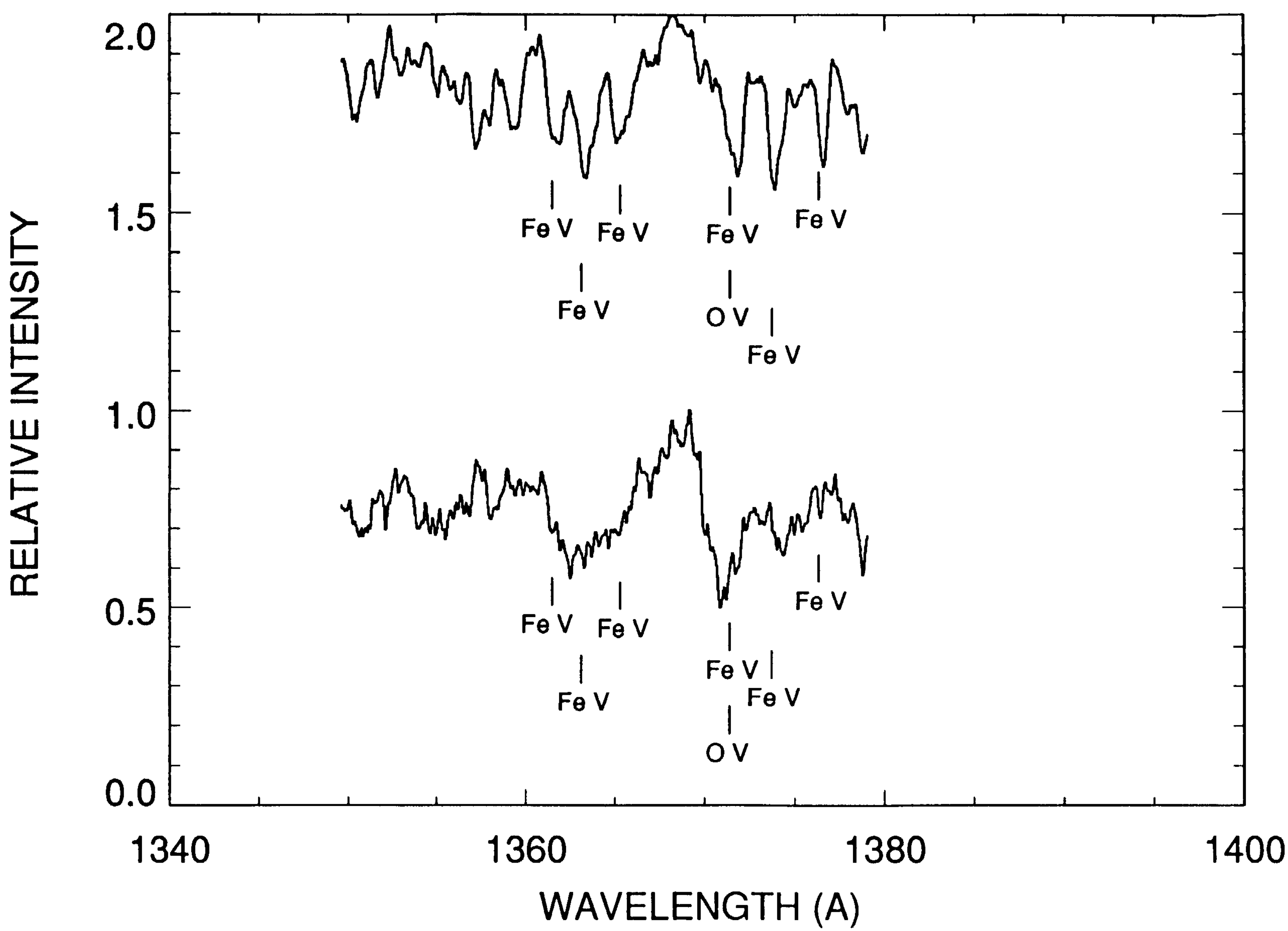

RELATIVE INTENSITY
2.0
1.5
1.0
0.5
0.0
Fe V
Fe V
Fe V
Fe V
Fe V
O V
Fe V
Fe V
Fe V
Fe V
Fe V
Fe V
Fe V
O V
1340
1360
1380
1400
WAVELENGTH (A)

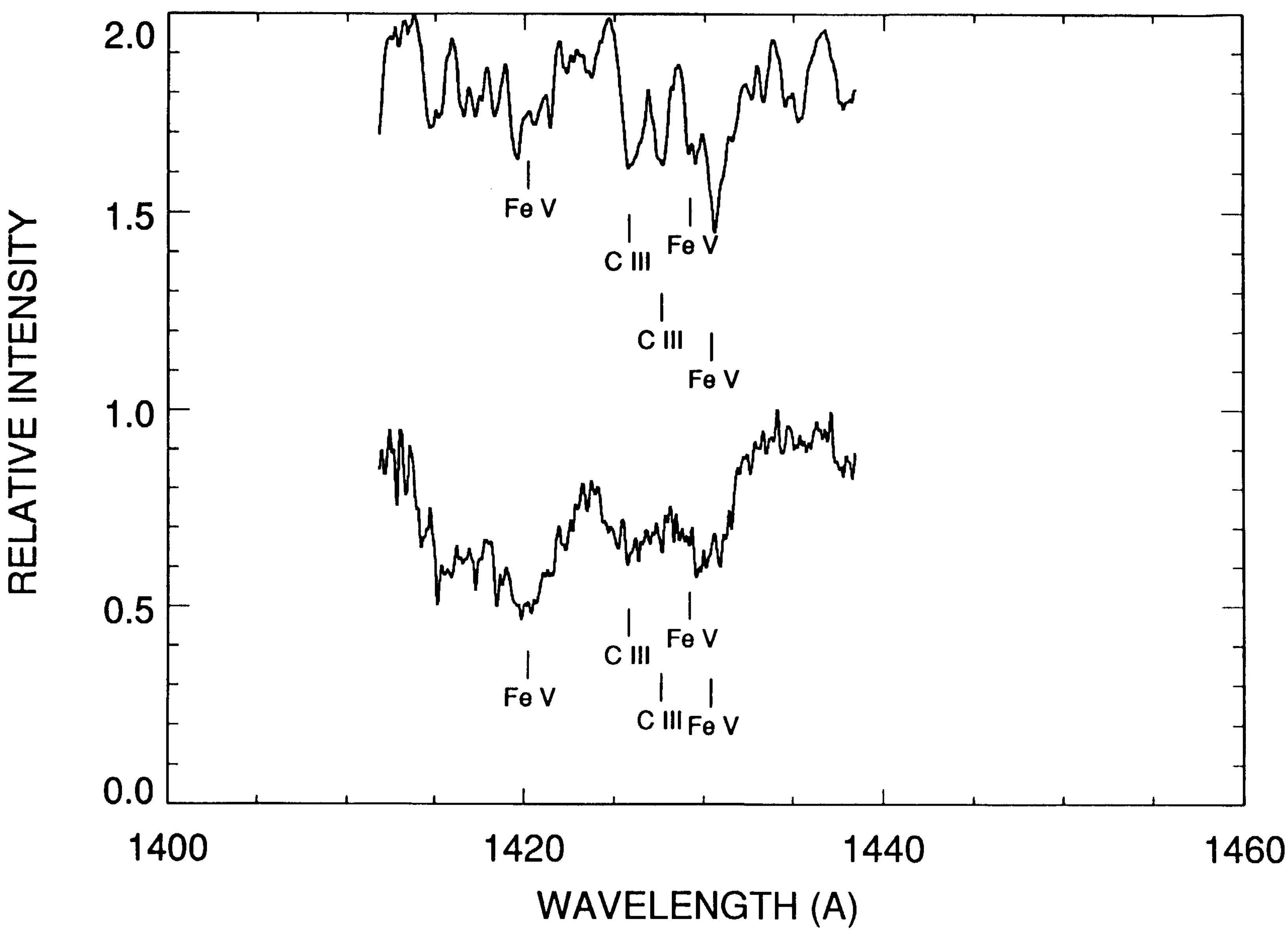

2.0
1.5
1.0
0.5
0.0
RELATIVE INTENSITY
Fe V
C III
Fe V
C III
Fe V
Fe V
C III
Fe V
C III
Fe V
1400
1420
1440
1460
WAVELENGTH (A)

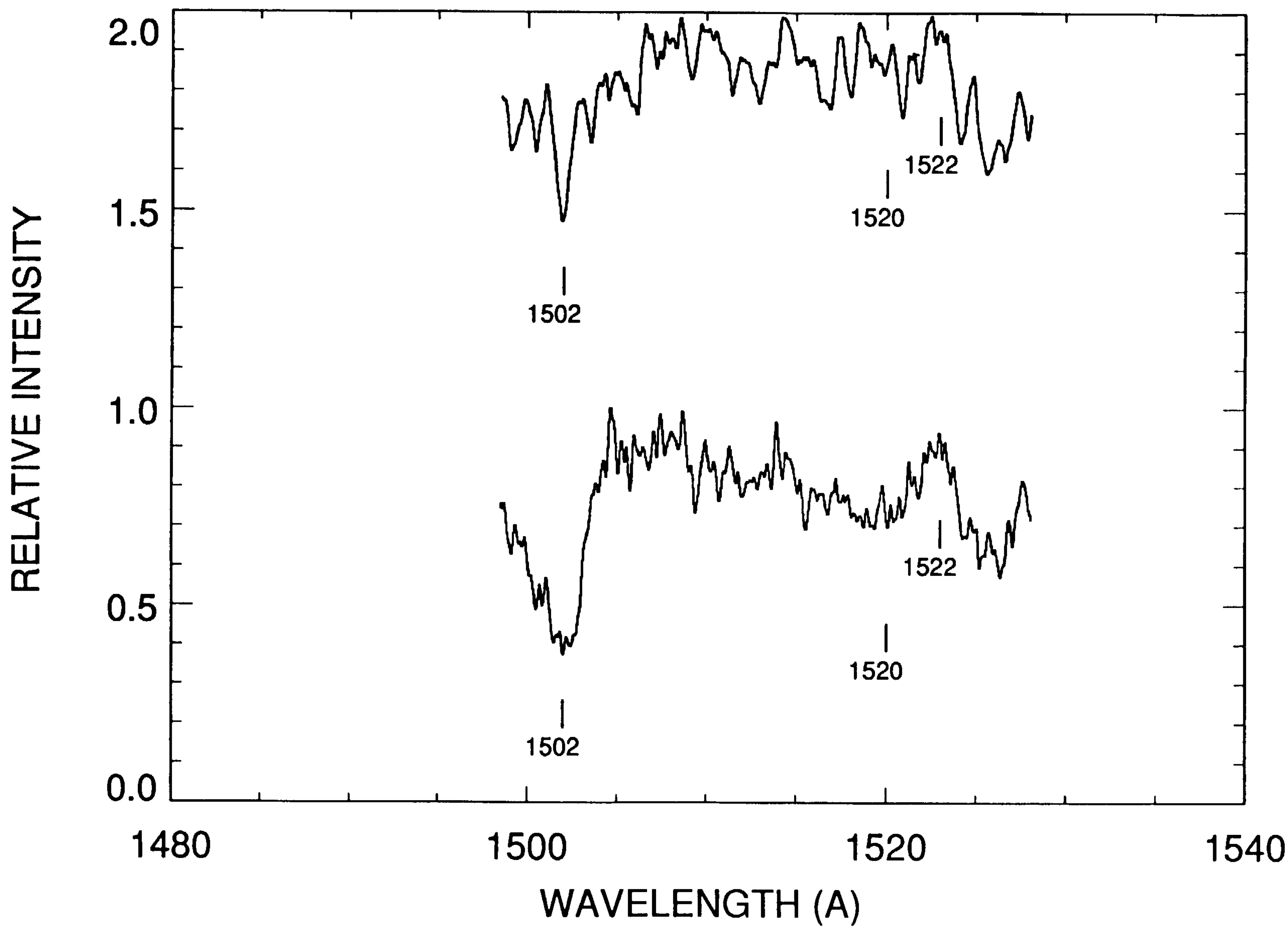
2.0
1.5
1.0
0.5
0.0
RELATIVE INTENSITY
1480
1500
1520
1540
WAVELENGTH (A)
1502
1520
1522
1502
1520
1522

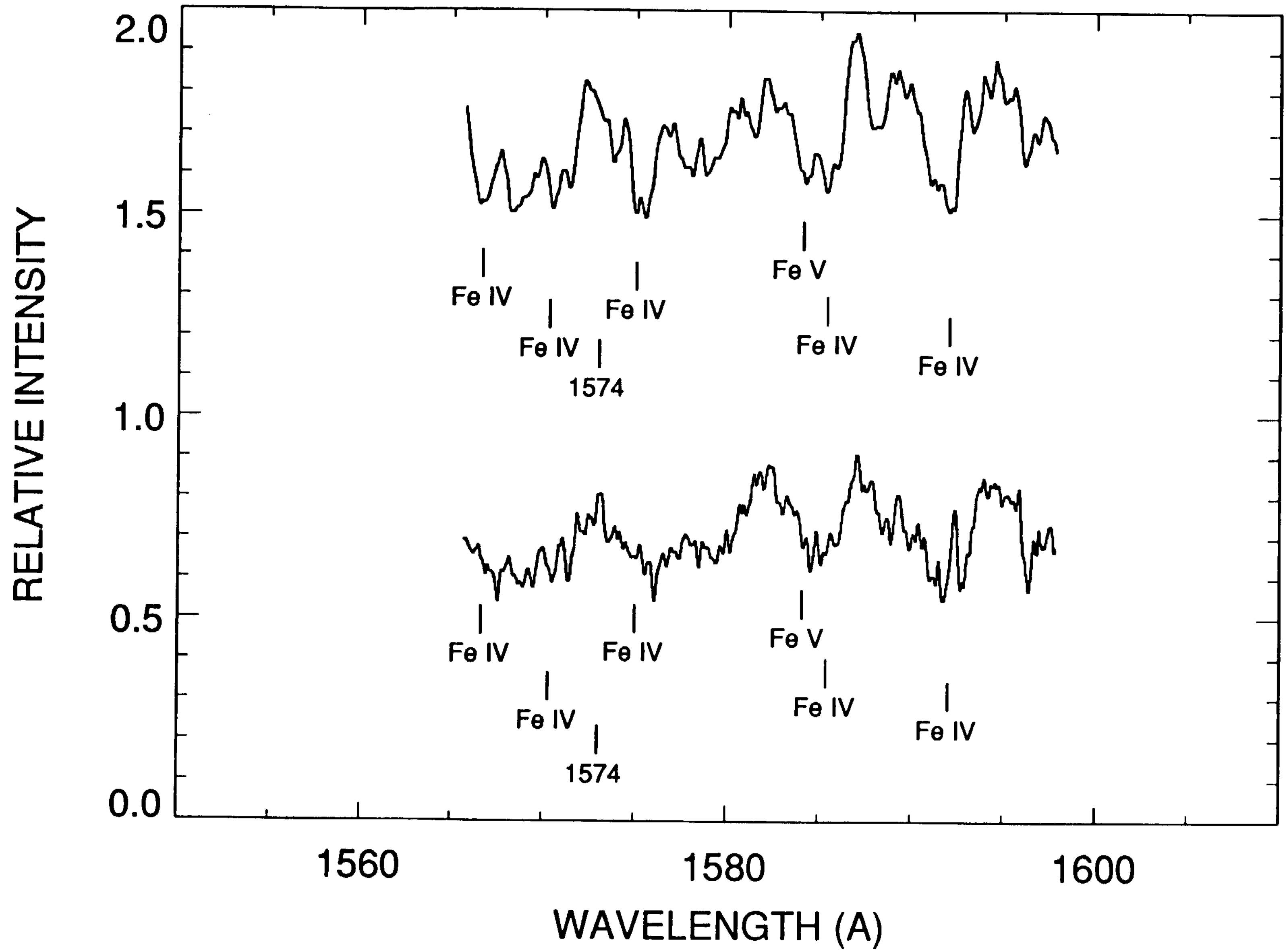
RELATIVE INTENSITY
2.0
1.5
1.0
0.5
0.0
WAVELENGTH (A)
1560
1580
1600
Fe IV
Fe IV
1574
Fe IV
Fe V
Fe IV
Fe IV
Fe IV
Fe IV
1574
Fe IV
Fe V
Fe IV
Fe IV

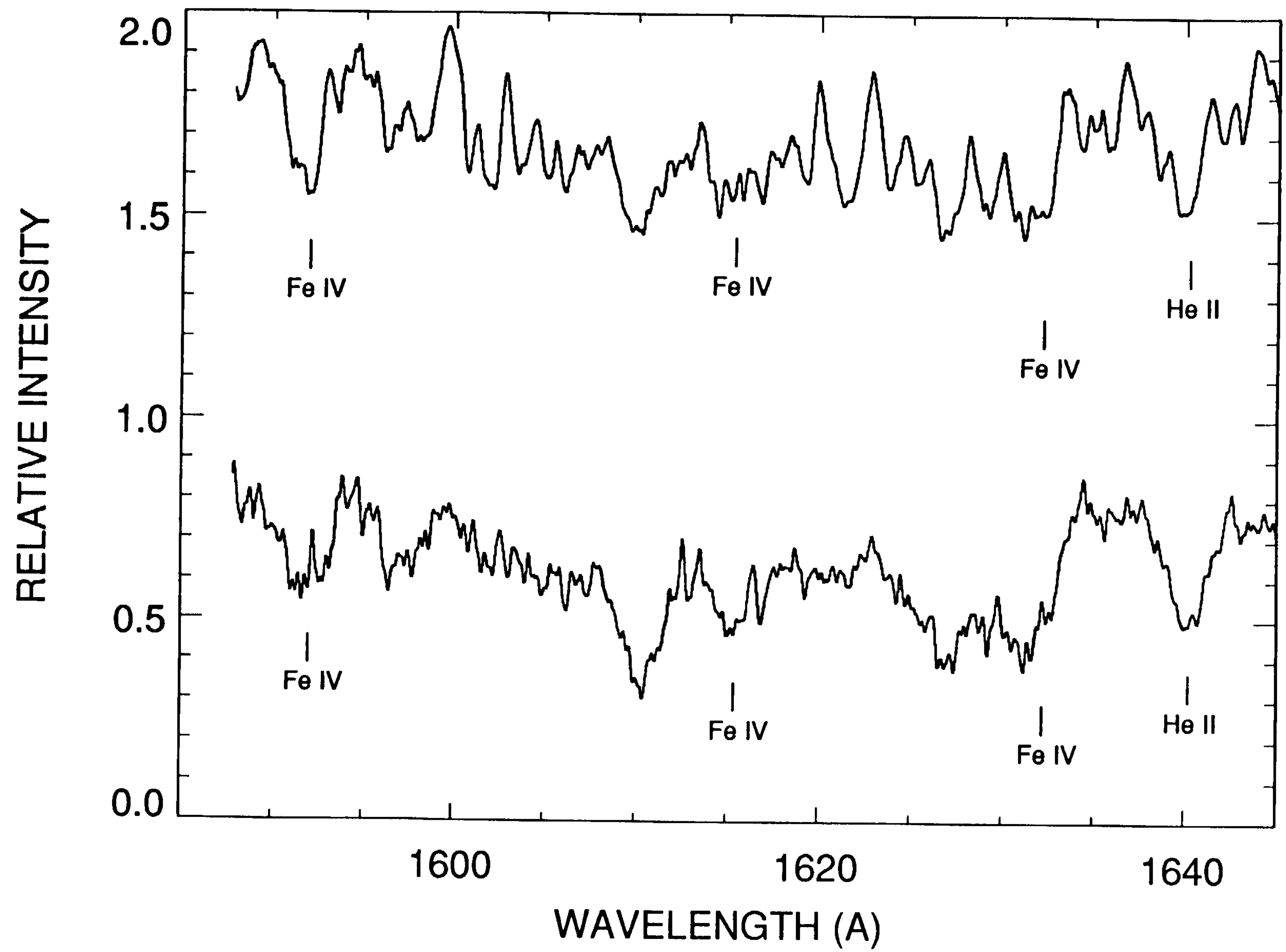

2.0
1.5
1.0
0.5
0.0
RELATIVE INTENSITY
Fe IV
Fe IV
Fe IV
He II
Fe IV
Fe IV
Fe IV
He II
1600
1620
1640
WAVELENGTH (A)

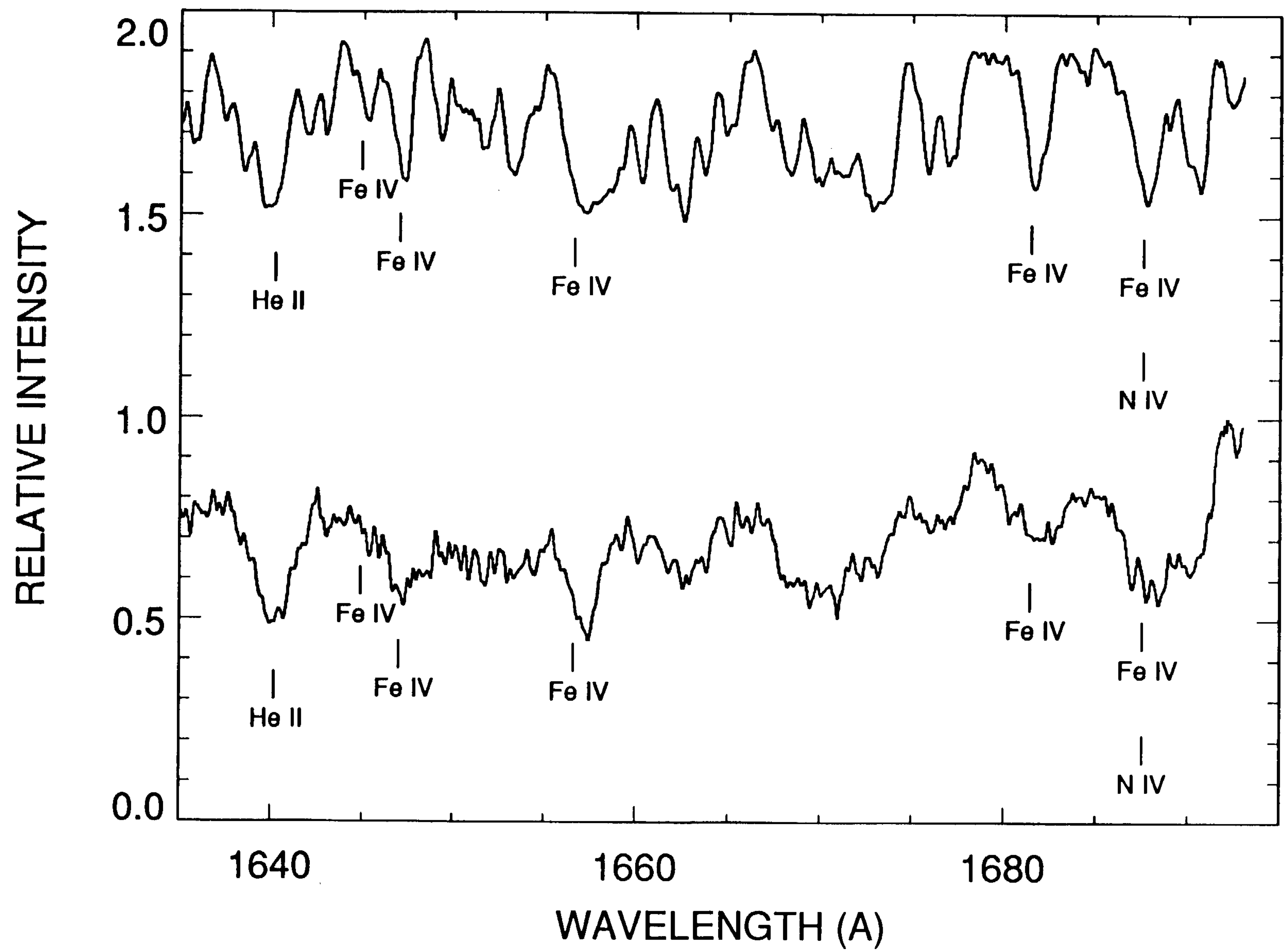
RELATIVE INTENSITY
2.0
1.5
1.0
0.5
0.0
He II
Fe IV
Fe IV
Fe IV
Fe IV
Fe IV
N IV
He II
Fe IV
Fe IV
Fe IV
Fe IV
Fe IV
N IV
1640
1660
1680
WAVELENGTH (A)

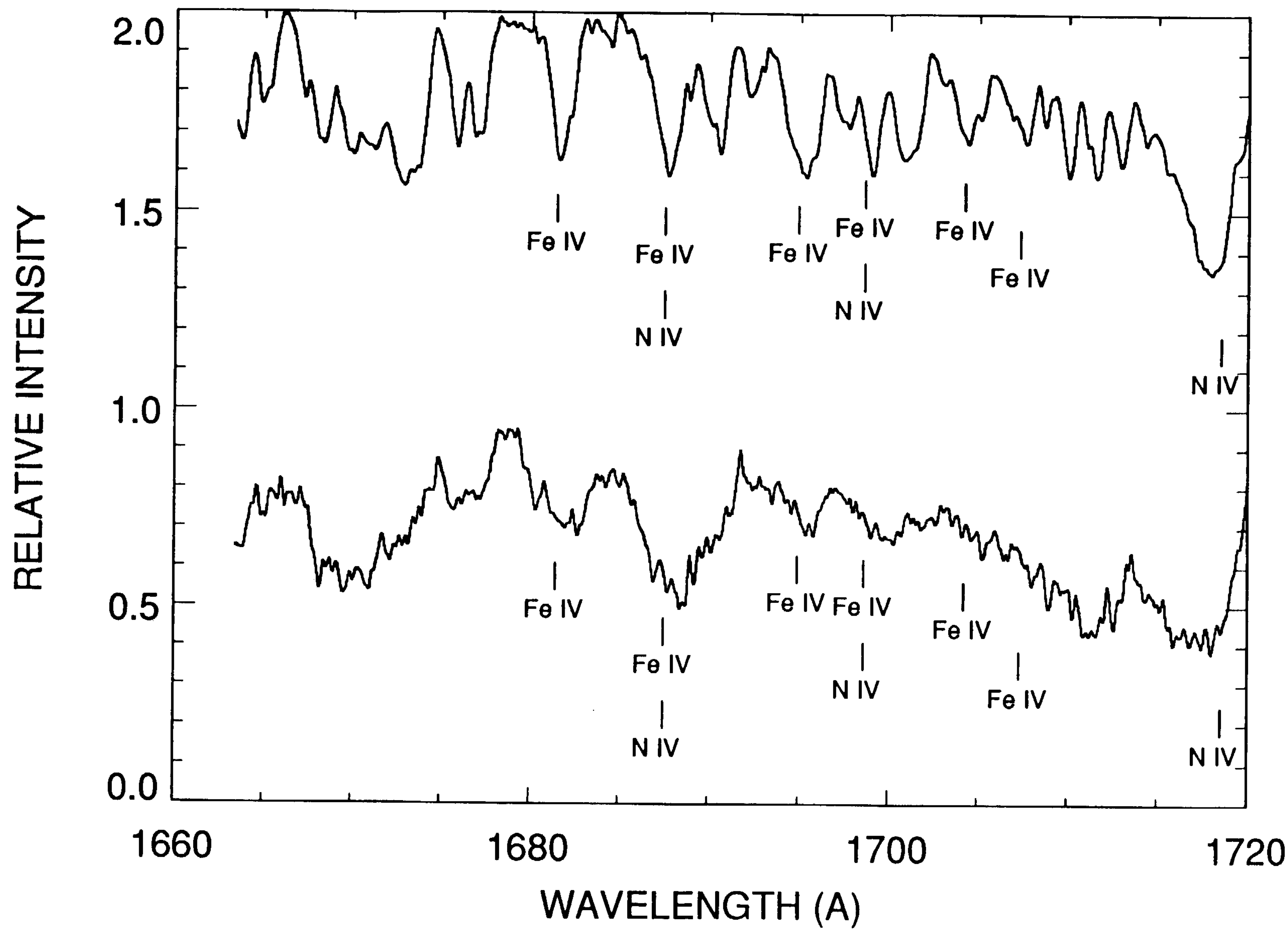

RELATIVE INTENSITY
WAVELENGTH (A)
2.0
1.5
1.0
0.5
0.0
1660
1680
1700
1720
Fe IV
N IV

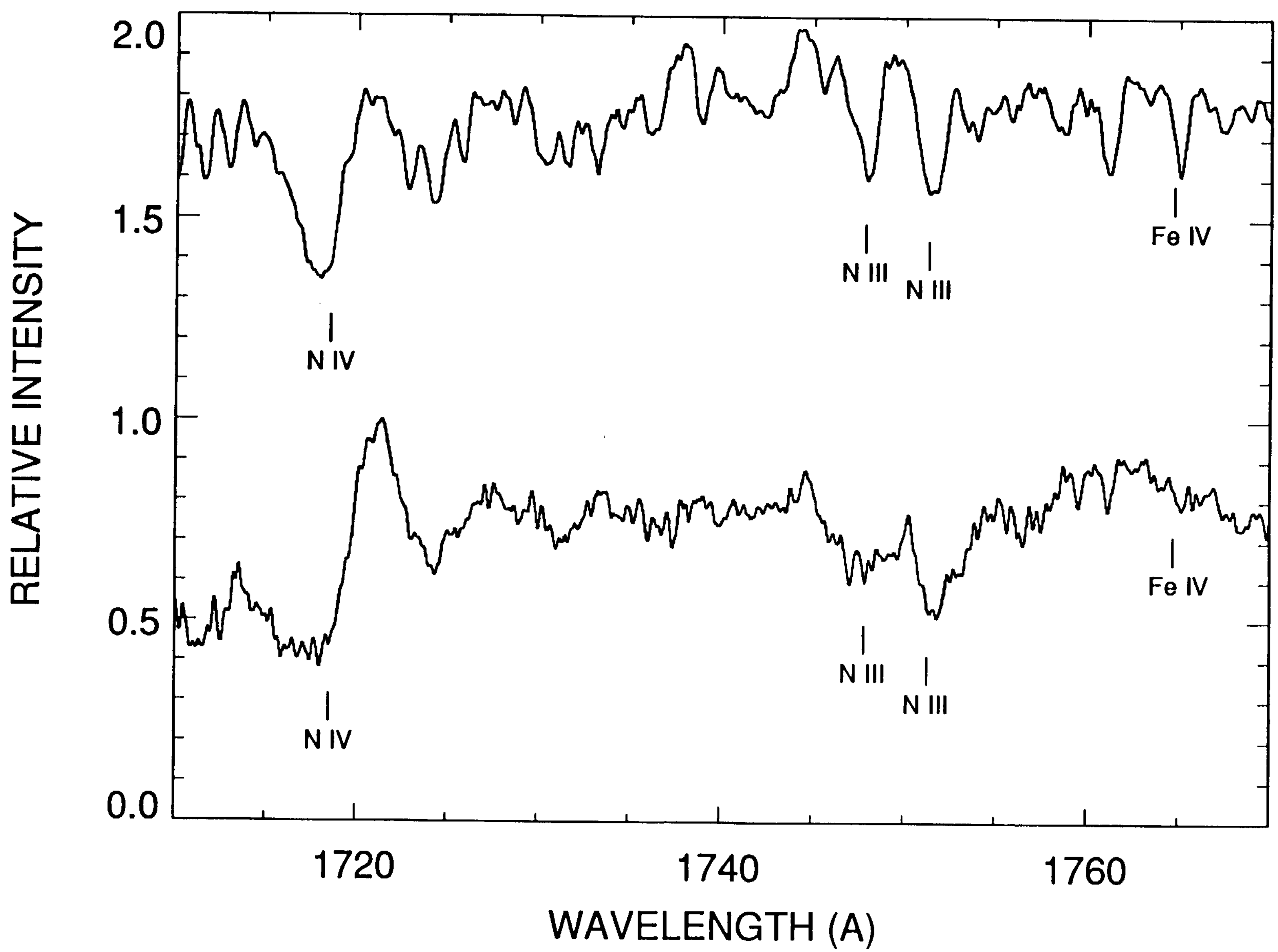

2.0
1.5
1.0
0.5
0.0
RELATIVE INTENSITY
N IV
N III
N III
Fe IV
N IV
N III
N III
Fe IV
1720
1740
1760
WAVELENGTH (A)

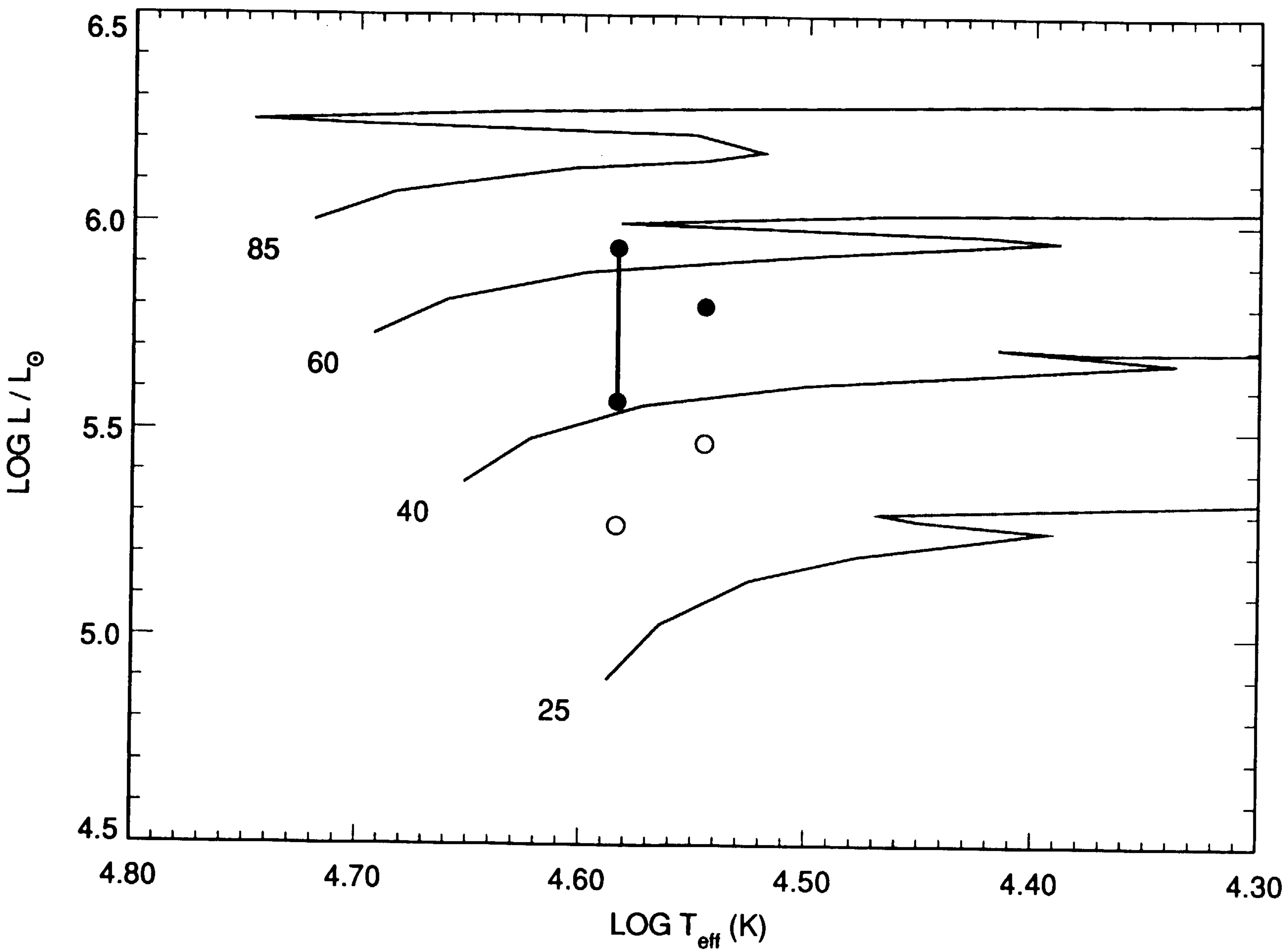

6.5
6.0
5.5
5.0
4.5
LOG L / L$_\odot$
4.80
4.70
4.60
4.50
4.40
4.30
LOG T$_{eff}$ (K)
85
60
40
25